I&EC research
Industrial & Engineering Chemistry Research

Article

pubs.acs.org/IECR

Magnetic Nanocarbon Adsorbents with Enhanced Hexavalent Chromium Removal: Morphology Dependence of Fibrillar vs Particulate Structures

Jiangnan Huang,[†,§] Yonghai Cao,[*,†,§] Qian Shao,[∥] Xiangfang Peng,[†] and Zhanhu Guo[*,‡]

[†]School of Mechanical & Automotive Engineering, South China University of Technology, Guangzhou, Guangdong 510640, China

[‡]Integrated Composites Laboratory (ICL), Department of Chemical and Biomolecular Engineering, University of Tennessee, Knoxville, Tennessee 37996, United States

[§]School of Chemistry and Chemical Engineering, South China University of Technology, Guangzhou, Guangdong 510640, China

[∥]College of Chemical and Environmental Engineering, Shandong University of Science and Technology, Qingdao 266590, P. R. China

Supporting Information

ABSTRACT: Fibrillar and particulate structure magnetic carbons (MCFs and MCPs) were prepared from the same precursor (polyacrylonitrile and $Fe(NO_3)_3{\cdot}9H_2O$) by using a different method, displaying a significant morphology dependence on wastewater treatment. TEM, SEM, XPS, TGA, etc. were systematically carried out to characterize the carbon samples to verify the morphology difference between these two kinds of carbon adsorbents. The results demonstrated that, along with the increase of the $Fe(NO_3)_3{\cdot}9H_2O$ loading in the precursor from 10 to 40 wt %, the fibrillar nanoadsorbents displayed an improved activity from 12.6% to 51.4% Cr(VI) removal percentage with the initial Cr(VI) concentration at 4 mg/L. For the maximum removal capacity, the fibrillar sample (MCFs-40) demonstrated 3 times higher removing capacity (43.17 mg/g) than that of particulate nanoadsorbents (MCPs-40, 15.88 mg/g) for the Cr(VI) removal with pH at 1, demonstrating that the fibrillar sample was more favorable for the wastewater treatment than particulate sample. This enhanced removal was mainly attributed to higher specific surface area of the fibrillar sample, leading to more active sites for the adsorption of Cr(VI) and produced Cr(III) ions. The chemical adsorption of Cr(VI) ions over two kinds of adsorbents were disclosed in this removal process. There was a good stability of 5 recycles for the Cr(VI) removal in the neutral solution over MCFs-40 (about 1.4 mg/g) and MCPs-40 (about 0.41 mg/g) with initial Cr(VI) concentration at 4 mg/L. This work can provide an understanding for the rational design of adsorbent in wastewater treatment.

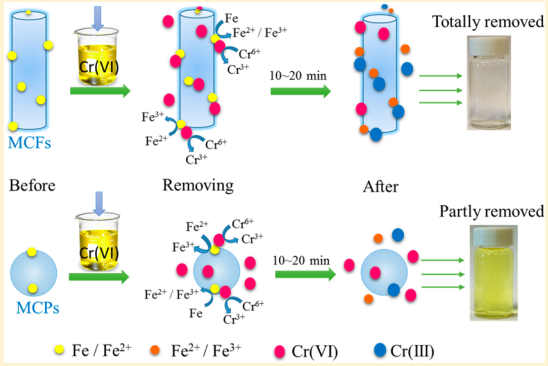

1. INTRODUCTION

Because of the rapid development of manufacturing, the social environment faces more and more serious problems all over the world. The quality of water is continuously deteriorating due to its increasing toxic threat to humans and the environment.[1−6] A lot of pollutants, such as dyes and organic/inorganic contaminants, were observed in the wastewater.[7−24] To avoid these various pollutants in the water, many technologies were developed, for instance, catalytic degradation, filtration, electrotransformation, and adsorption.[25−43] For the disposal of inorganic contaminants, several kinds of toxic metal ions, e.g., Cr(VI), Cu(II), Cd(II), As(II), Hg(II), etc., were observed in the wastewater.[44] Among those metal ions, the Cr(VI) ion, causing liver damage, carcinogenic effects, and inherited gene defects in human, is a typical contaminant with its wide industrial applications. Therefore, it is crucial to remove Cr(VI) ions from the wastewater due to its high toxicity and mobility.[45] Recently, the adsorption method is reported as an effective method to remove Cr(VI) ions from the polluted waters.[46] Numerous adsorbents, such as biosorbents, clay minerals, metal phosphates, zeolites, activated carbon, and magnetic carbons, were developed to advance the progress of wastewater treatment.[47−52] In the case of magnetic carbons, so far, more and more intensive attention has been attracted in the academia community, due to their highly porous structure with facile-controlled chemical properties and magnetization for easy separation.[51,53]

There were two steps for the Cr(VI) removal process over the magnetic carbons: adsorption and redox reaction. The Cr(VI) ions first were adsorbed on the surface of adsorbents through electrostatic interaction, and then the adsorbed Cr(VI)

Received: July 10, 2017
Revised: August 15, 2017
Accepted: August 30, 2017
Published: August 30, 2017

DOI: 10.1021/acs.iecr.7b02835
Ind. Eng. Chem. Res. 2017, 56, 10689−10701

ions reacted with the magnetic nanoparticles, which were synthesized from the annealing process, to produce the Cr(III) ions through a redox reaction (eq 1).[54] In this process, Fe^0 and Fe^{2+} nanoparticles were considered to be potential adsorbents for Cr(VI) removal since they can be used as a reducing agent.[55] The produced Cr(III) ions, considered as an essential nutrient requirement for sugar and fat metabolism in human bodies, are nontoxic.[56] In the neutral solution, the magnetic carbon can adsorb the Cr(VI) ions and a small part of Cr(VI) ions was reduced to Cr(III). In contrast, in the acid solution, the oxidability of Cr(VI) ions was enhanced due to the abundant of H^+ ions and the reduction reaction between the Cr(VI) and Fe^0 and Fe^{2+} nanoparticles was enhanced subsequently to produce more Cr(III) ions.[57,58] Therefore, both routes (adsorption and reduction reaction) are very important in Cr(VI) removal.

$$CrO_4^{2-} + 8H^+ + 3e^- \rightarrow Cr^{3+} + 4H_2O \quad (1)$$

Herein, a lot of research work focusing on the magnetic carbon adsorbents demonstrated that magnetic carbons could be applied as alternative adsorbents for Cr(VI) removal.[59] These carbon-based materials with many surface functional groups (hydroxyl −OH, carboxyl −COOH, and carbonyl C═O) and a high proportion of the sp^2 carbon region not only reduced Cr(VI) to Cr(III) ions[45,60] but also introduced and dispersed the iron and iron oxide nanoparticles in their matrix very well, thereby significantly enhancing the adsorption capacity.[61] Among those magnetic carbons, two main kinds of morphology categories, e.g., fibrillar and particulate adsorbent, were widely investigated. Carbon fibers, well-known to have large specific surface area and high adsorption capacity, were profusely used as typical fibrillar adsorbents for pollution control.[62−64] For instance, Zheng et al. synthesized the porous carbon fibers with strong anion-exchangeable functional groups, displaying superior performance in the removal of trace Cr(VI) down to ppb levels at natural pH with rapid kinetics.[62] Furthermore, the hybrid strong anion exchange porous carbon fiber showed a stable and regenerable performance for adsorbing and converting Cr(VI) into Cr(III) with no change in pH, which is attributed to the catalytic activity of surface oxygen functional groups.[63] Huang et al. found that the activated carbon fiber with stabilized nanoscale zerovalent irons (NZVI) demonstrated impressive performance in Cr(VI) removal, and they believed that NZVI loaded on the surface was partial oxidized, and the removal of Cr(VI) was attributed to the adsorption of fibrillar adsorbents and its reducibility.[65] Particulate magnetic carbon adsorbents were also intensively studied in wastewater treatment over the past several years. The carbon layer prevents iron from dissolving in the acidic solutions, leading to a longer lifetime of the adsorbents for the recyling.[66] Zhang et al. synthesized the magnetic hollow carbon nanospheres for Cr(VI) removal, demonstrating high removal capacity (200 mg/g).[67] They claimed that the abundant functional groups and the enhanced electrostatic interactions between π electrons and Cr species would facilitate the removal rate.[67] Zhu et al. prepared magnetic carbons by using microwave energy-assisted pyrolysis and used as adsorbent in Cr(VI) removal.[55,68] Qiu et al. reported that the magnetic carbons synthesized from glucose and $Fe(NO_3)_3{\cdot}9H_2O$ can be used as adsorbents in Cr(VI) removal with high removal capacity (293.8 mg/g).[53,69] Furthermore, heteroatom doped carbons with a particulate structure were also developed to improve the removal efficiency.[57,58] Although this research displayed diverse removal capacity over magnetic carbons in Cr(VI) removal, the intrinsic influence of the magnetic carbons with different morphologies was still not well-defined. From the point of fundamental understanding, verifying the better performance on the different morphology is a significant issue in the adsorbent design and optimization of process. Meanwhile, there are very few works focused on the morphology effect of materials synthesized by different processes with the same precursors on the Cr(VI) removal. Therefore, in this study, we have synthesized the different morphologies of adsorbents based on the same precursors and the same amount of metal salt to verify the significant influence on the Cr(VI) removal.

In the present work, the magnetic carbons with different morphologies (fibrillar and particulate carbons), which were prepared by the same precursors (polyacrylonitrile (PAN) and $Fe(NO_3)_3{\cdot}9H_2O$), were used as adsorbents for Cr(VI) removal in neutral and acid solutions. SEM, XRD, BET, XPS, and other techniques were used to study the influence of different morphologies and composition of the prepared materials on Cr(VI) removal. Different Cr(VI) removal mechanisms of the prepared adsorbents were proposed for treating the pollutant water in acid and neutral conditions. The magnetic carbons displayed high efficiency in Cr(VI) removal, combining with adsorption and redox reaction.

2. EXPERIMENTAL SECTION

2.1. Materials. PAN powders (M_W = 150 000, Scientific Polymer Products, Inc.) was used as the carbon source. Iron(III) nitrate nonahydrate ($Fe(NO_3)_3{\cdot}9H_2O$, reagent ACS) was obtained from Acros Organics. *N*,*N*-Dimethylformamide (DMF, anhydrous, 99.8%) with a density of 0.94 g/mL was purchased from Sigma-Aldrich. Sodium hydroxide (NaOH, 99.1%), hydrochloric acid (HCl, 95%), potassium dichromate ($K_2Cr_2O_7$), and 1,5-diphenylacarbazide (DPC) were obtained from Alfa Aesar company. Phosphoric acid (H_3PO_4, 85 wt %) was purchased from Fisher Scientific. All of the chemicals were used without any treatments.

2.2. Synthesis of Magnetic Carbon Fibrillar and Particulate Nanoadsorbents. *2.2.1. Magnetic Carbon Fibrillar Nanoadsorbents.* A certain weight of PAN (1.64 g) and $Fe(NO_3)_3{\cdot}9H_2O$ (10, 20, 30, and 40 wt %) was dissolved in 20 mL of DMF. In order to prepare the PAN/$Fe(NO_3)_3$/DMF solution, the suspensions were stirred vigorously by a magnetic stirrer at room temperature until the solution was homogeneously mixed. Then the solution was used for electrospinning by using a syringe pump. After the electrospun PAN/$Fe(NO_3)_3$ fibers went out of the needle, the fibers were collected by grounded aluminum foils. The processing parameters were shown as follows: 20.0 kV (high voltage), 6.0 μL/min (feeding flowing speed), and 12 cm (distance from needle to the collector). Then the fibers were dried at 60 °C in the oven overnight for the solvent evaporation. After that, the electrospun fibers were put into the ceramic tube in the furnace and stabilized under an air circumstance at 250 °C for 1 h, with a heating rate at 2 °C min^{-1} from room temperature. Subsequently, the stabilized fibers were carbonized at 800 °C for 2 h in nitrogen atmosphere with a heating rate of 10 °C min^{-1} to obtain magnetic carbon fibers. The sample names of MCFs-10, MCFs-20, MCFs-30, and MCFs-40 represented the magnetic carbon fibers, in which the loadings of $Fe(NO_3)_3{\cdot}9H_2O$ in the precursors were 10, 20, 30, and 40 wt %, respectively. Furthermore, the higher loading of $Fe(NO_3)_3{\cdot}9H_2O$ in the precursor caused serious electro-discharging

DOI: 10.1021/acs.iecr.7b02835
Ind. Eng. Chem. Res. 2017, 56, 10689−10701

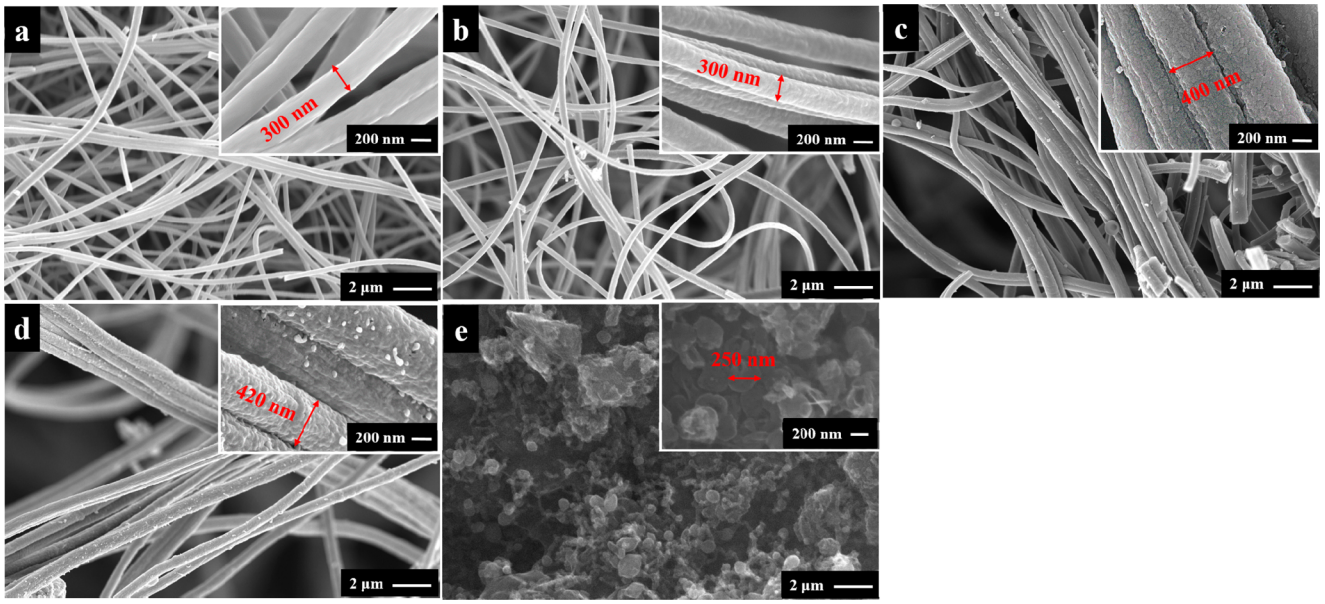

Figure 1. Typical low magnification SEM images of the synthesized fibrillar and particulate magnetic carbons: (a) MCFs-10, (b) MCFs-20, (c) MCFs-30, (d) MCFs-40, and (e) MCPs-40. The high magnification SEM images can be found in the inset images for each sample.

during the electrospinning and could not obtain fibers. Therefore, the properties and performance of MCFs and MCPs with >40 wt % loading of $Fe(NO_3)_3{\cdot}9H_2O$ were not investigated in this work.

2.2.2. Magnetic Carbon Particulate Nanoadsorbents. PAN (1.64 g) and $Fe(NO_3)_3{\cdot}9H_2O$ (40 wt %) were mixed in DMF solution, and then the mixture was treated under ultrasonication for 2 h to prepare a uniform mixture. After that, the mixture was dried at 110 °C overnight to evaporate the solvent. The obtained powder samples were then carbonized at 800 °C for 2 h under nitrogen atmosphere. Then the samples were grinded into fine powders, which were noted as MCPs-40.

2.3. Characterizations. The transmission electron microscope (TEM) images were observed by a FEI Tecnai G2 12 microscope operated at 100 kV and a JEOL JEM2010 microscope operated at 200 kV. The specimens for TEM were prepared by ultrasonically suspending the sample in acetone and depositing a drop of the suspension onto a grid. The scanning electron microscope (SEM) images were obtained by a LEO 1530VP electron microscope. Brunauer–Emmett–Teller (BET) specific surface areas, pore volumes, and pore size were measured by N_2 adsorption at liquid N_2 temperature in a Micromeretics Gemini. X-ray diffraction (XRD) patterns were recorded on a Bruker D8 Advance diffractometer equipped with a rotating anode using Cu Kα radiation (40 kV, 40 mA). The Raman spectra were obtained in Acton TriVista 555 Raman spectrometer with an excitation wavelength at 532 nm with 150 μm spot size. X-ray photoelectron spectroscopy (XPS) spectra were performed in a Kratos Axis ultra (DLD) spectrometer equipped with an Al Kα X-ray source in ultrahigh vacuum (UHV; $<10^{-10}$ Torr). The surfaces of samples were cleaned by heat treatment at 100 °C in UHV prior to the measurements. The TGA experiments were operated by Q-500 TA Instruments, and the fresh and treated samples were heated from 25 to 800 °C at a heating rate and air flow rate of 10 °C/min and 20 mL/min, respectively.

2.4. Cr(VI) Removal Performance. All of the experiments were carried out in a 50 mL beaker containing 20 mL of Cr(VI) solution at room temperature (25 °C) similar to our previous work.[53] Typically, a certain weight of magnetic carbon particles and fibers was added into the Cr(VI) solution. In order to disperse the adsorbents and supply enough adsorption time, the suspension liquid with adsorbents was treated under ultrasonication (300 W, KQ-300DE, Kunshan ultrasonic instrument co., Ltd.) for a certain time at room temperature, since the rated power has a strong influence on the Cr(VI) removal efficiency.[70,71] The effects of adsorbents type (MCFs-10, MCFs-20, MCFs-30, MCFs-40, and MCPs-40), initial Cr(VI) concentration (1.0–10.0 mg/L), treatment time (2.5–20.0 min), the dosage of adsorbents (0.5–5 g/L), and pH value of Cr(VI) solutions (1.0–11.0) measured by a pH meter (Vernier Lab Quest with pH-BTA sensor) on the Cr(VI) removal efficiency and capacity were investigated in this work. The HCl solution (1 mol/L) and NaOH (1 mol/L) were used to adjust the solution pH value. For kinetic study, the synthesized magnetic carbons were used to treat different concentrations of Cr(VI) solution (20.0 mL) at initial pH values of 1.0 and 7.0, respectively. The Cr(VI) concentrations that remained in solutions were measured at different interval times. The Cr(VI) concentration in solution was measured by the colorimetric method[7] by using the obtained standard fitting (eq 2):

$$C_e = 3.8716A - 0.00039 \tag{2}$$

where C_e is the concentration of Cr(VI) and A is the absorbance at 540 nm obtained from the UV–vis test.

The Cr(VI) removal percentage (R%) was calculated using eq 3:

$$R\% = \frac{(C_0 - C_e)}{C_0} \times 100\% \tag{3}$$

where C_0 and C_e (mg L^{-1}) are the Cr(VI) concentrations in solution before and after treatment, respectively. The removal capacity (q_e, mg g^{-1}) is quantified by eq 4:

$$q_e = \frac{(C_0 - C_e)}{m} V \tag{4}$$

DOI: 10.1021/acs.iecr.7b02835
Ind. Eng. Chem. Res. 2017, 56, 10689–10701

where V (L) represents the volume of Cr(VI) solution and m (g) is the mass of the used magnetic carbon nanoadsorbents.

In this work, the data utilized to fit the pseudo-second kinetic model was obtained from the average of the integrated results three replicates to make the results more reliable.

3. RESULTS AND DISCUSSION

3.1. Morphology Study. Figure 1 shows the typical morphology of the as-synthesized samples. From Figure 1a−e, all of the obtained magnetic carbon fibers display a regular uniform fiber structure. The diameter of MCFs ranged at about 230−420 nm with the loading of $Fe(NO_3)_3{\cdot}9H_2O$ in their precursors from 10 to 40 wt % (Figure 1a−d), which was also observed over the fiber samples fabricated by PAN and iron acetylacetonate.[72,73] The tiny increase of diameters in those fiber samples was probably ascribed to the cooperation of $Fe(NO_3)_3{\cdot}9H_2O$, which increased the viscosity of precursor solutions during the electrospinning process.[74,75] The viscosity of solutions plays a significant role in the formation of fibers during the electrospinning process. Zong et al. found that the solution viscosity was one of the most effective variables to control the fiber morphology.[76] Tan et al. also reported that it was impotent to reach a sufficient level of solution viscosity to produce a uniform jet during electrospinning and restrain effects of surface tension, which plays a significant role in bead formation on electrospun nanofibers.[77] For the magnetic carbon particles, the diameter of MCPs-40 was about 250 nm (Figure 1d). It was clearly observed that the number of nanoparticles on the MCFs surface increased with the increase of the $Fe(NO_3)_3{\cdot}9H_2O$ loading from 10 to 40 wt %. According to the TEM images in Figure 2a, the in situ formed nanoparticles with the graphite shell and Fe core were well dispersed over the carbon fibers.[72,73] What was more, the carbon encapsulated Fe nanoparticles through the carbon fibers displayed a broad size distribution with the diameter ranging from 50 to 150 nm. Meanwhile, relative uniform Fe−C core−shell nanoparticles (with diameter range of 50−10 nm) and a little of carbon sheet were observed in the magnetic carbon particles (MCPs-40) as well (Figure 2c,d).

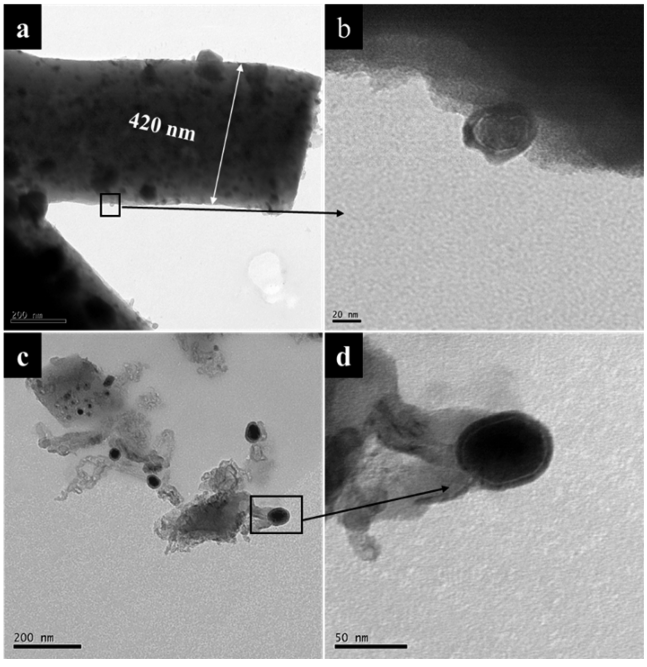

Figure 2. Typical TEM images of the synthesized fibrillar and particulate magnetic carbons: (a and b) MCFs-40 and (c and d) MCPs-40.

3.2. Material Phases, Defects Degree, and Surface Chemical Elements Analysis. XRD, Raman, and XPS were applied to analyze the crystalline structures of materials, defects degrees of carbon, and surface elements of the prepared samples. Figure 3a presents the XRD patterns of the synthesized MCFs and MCPs-40. The diffraction peak at 26.4° indicated the (002) planes of graphite-2H, while the peaks at 40.5°, 44.6°, 42.7°, and 49.7° corresponded to the [100] plane of FeO, the [110] plane of α-Fe, and the [111] and [200] planes of γ-Fe, respectively.[78] The rest of the diffraction peaks at 37.6°, 39.8°, 43.7°, 45.8°, 48.6°, and 51.8° demonstrated the presence of [121], [002], [102], [112], [131], and [122] planes of Fe_3C, respectively.[78] The content of FeO, Fe_3C, α-Fe, and γ-Fe nanoparticles in the magnetic carbon fibers increased alone with the increase of the $Fe(NO_3)_3{\cdot}9H_2O$ loading in MCFs precursors. It was worth noting that there was too little of the metal particles on the MCFs-10 surface to be detected (Figure S1 and Table S1).

Figure 3b shows the Raman spectra of MCFs and MCPs-40, which are used to evaluate the defects on the samples surface.[79] The ratio of the intensities of "disorder" or defective degree (the $R = I_D/I_G$) was measured.[79,80] The R depends on the in-plane graphitic crystallite size (L_a): $L_a = 4.4/R$.[81] As shown in Table S2, the positions of D and G peaks shifted slightly to a lower frequency with increasing the $Fe(NO_3)_3{\cdot}9H_2O$ loading in the MCFs precursors. The R ratio and L_a of MCFs displayed slightly changes since 10−30 wt % $Fe(NO_3)_3{\cdot}9H_2O$ was added. When the loading of $Fe(NO_3)_3{\cdot}9H_2O$ gradually increased up to 40 wt %, the R ratio of samples increased to about 1.34 while the L_a value decreased to 3.22 nm, indicating that the addition of iron or iron oxide caused more defects in the MCFs, thus decreasing the in-plane graphitic crystallite, subsequently. The reason for this result was that iron atoms probably reacted with carbon atoms to form Fe_3C during the carbonization, which cracked the C−C bond in the graphite skeleton.[82]

The chemical compositions of the carbon samples were measured by XPS (Figure S1). The XPS survey showed four main peaks, i.e., C_{1s} (~284.6 eV), N_{1s} (~399.4 eV), O_{1s} (~530.3 eV), and Fe_{2p} (~710.8 eV; Figure S1), demonstrating that Fe atoms were successfully incorporated into the samples during the synthetic processes. The N and Fe atoms on the samples surface came from the precursor of PAN and $Fe(NO_3)_3$, respectively. The deconvolution of Fe_{2p} was shown in Figure 4. The peaks at around 709.6, 711.6, and 723.5 eV, on the surface of MCFs-10 and MCFs-20, were assigned to FeO, Fe_2O_3, and Fe_3O_4, respectively.[83,84] Moreover, a new peak of Fe^0 (706.9 eV) was found in MCFs-30, MCFs-40, and MCPs-40, attributed to the reduction between the iron oxide and carbon atoms at 800 °C.[85] According to Table S1, the amount of Fe atoms on the sample surfaces did not change significantly with increasing the $Fe(NO_3)_3$ loading in their precursors, but the ratios of Fe, FeO, Fe_2O_3, and Fe_3O_4 were greatly changed (Table S3). From the EDS result (Table S4), it could be clearly observed that the amount of Fe element in the sample increased alone with the increasing of $Fe(NO_3)_3$ loading in their precursors. With respect to the fibers, the Fe content on the surface increased alone with the increase of the $Fe(NO_3)_3$ loading, from 0.001 to 7.838%. This phenomenon was also observed on the content of FeO species. During this

DOI: 10.1021/acs.iecr.7b02835
Ind. Eng. Chem. Res. 2017, 56, 10689−10701

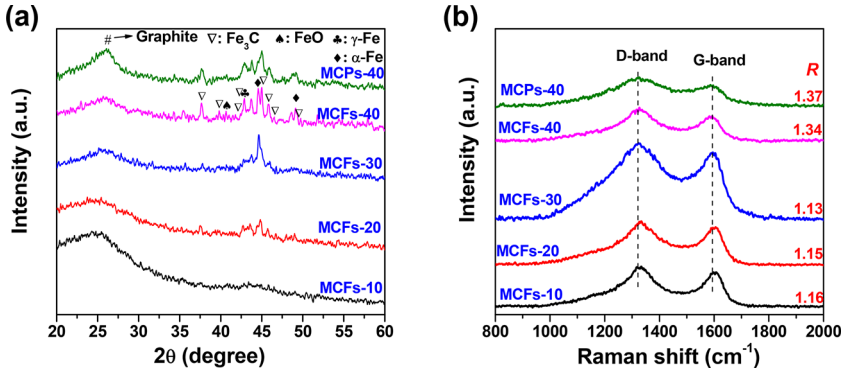

Figure 3. XRD patterns (a) and Raman spectra (b) of the synthesized fibrillar and particulate magnetic carbons.

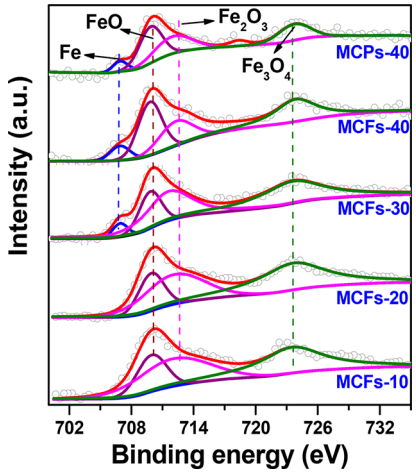

Figure 4. Fe 2p XPS spectra of the synthesized fibrillar and particulate magnetic carbons.

process, the content of Fe_2O_3 and Fe_3O_4 inversely varied, indicating that the Fe^0 or FeO nanoparticles were probably synthesized by the reduction of Fe_2O_3 and Fe_3O_4 with carbon atoms during the carbonization.[85]

3.4. Cr(VI) Removal Performance. The Cr(VI) removal efficiency and Cr(VI) removal capacity for the prepared magnetic carbon fibers and particles are shown in Figure 5. With the initial Cr(VI) concentration at 4 mg/L and pH at 7, MCFs-40 displayed a higher Cr(VI) removal efficiency than MCPs-40. The Cr(VI) removal efficiency and capacity of MCFs-40 are almost three times higher than those of MCPs-40, probable due to higher specific surface areas over MCFs-40 (Figure S2 and Table S5), providing more active sites for Cr(VI) removal. For the MCFs, the Cr(VI) removal efficiency was improved with the increase of the Fe salt loading, attributed to the reduction between the produced Fe^0 nanoparticles and Cr(VI) ions.[51,53,55,69] According to the reported literature and our previous work, the N element truly displayed a significant role for the Cr(VI) removal.[57,86] However, in the current work, we found that when we adjusted the N element content the removal efficiency did not vary as we thought. The intrinsic role of N element on the Cr(VI) removal is still under investigation and some results will be published in a dedicated paper in the future.

Figure 6a shows the effect of Cr(VI) concentration on the Cr(VI) removal performance. A complete Cr (VI) removal was observed in the case of using 2.5 g/L MCFs-40 in 20 mL of Cr(VI) solution (1.0 mg/L), while only 29.3% Cr(VI) was removed by 2.5 g/L MCPs-40 in the same condition. When the concentration of the Cr(VI) solution was increased, the Cr(VI) removal capacities of MCFs-40 and MCPs-40 were enhanced, since the collisions between the Cr(VI) ions and active sites were enhanced, resulting in a greater amount of Cr(VI) ions being adsorbed or reacted on the adsorbent surface.[57] In this process, the Cr(VI) efficiency and capacity of MCFs-40 were about 4.7 and 4.4 times higher than those of MCPs-40 in the 10.0 mg/L Cr(VI) solution, respectively. The contact time of absorbing Cr(VI) displayed a tiny effect on the Cr(VI) removal properties (Figure 6b). When the contact time increased from 2.5 to 20 min, the removal rate of Cr(VI) ions became slower,

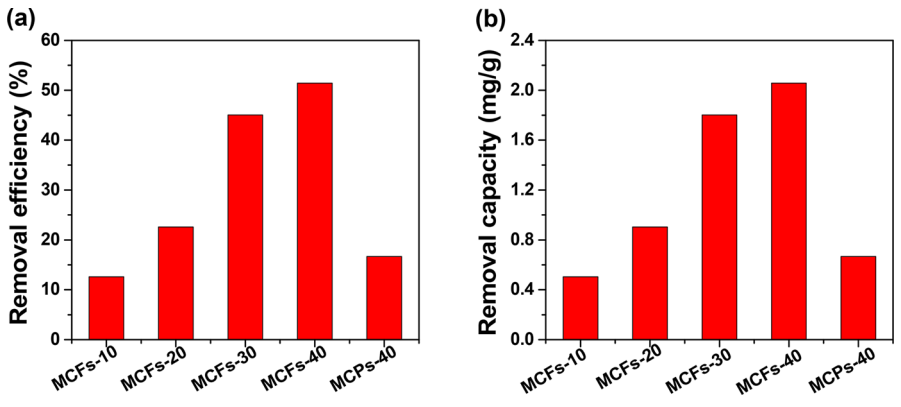

Figure 5. Cr(VI) removal efficiency (a) and Cr(VI) removal capacity (b) of the synthesized fibrillar and particulate magnetic carbons. The experiment conditions: 0.5 g/L adsorbents, 4 mg/L Cr(VI), pH 7, and ultrasonic treatment for 10 min.

DOI: 10.1021/acs.iecr.7b02835
Ind. Eng. Chem. Res. 2017, 56, 10689−10701

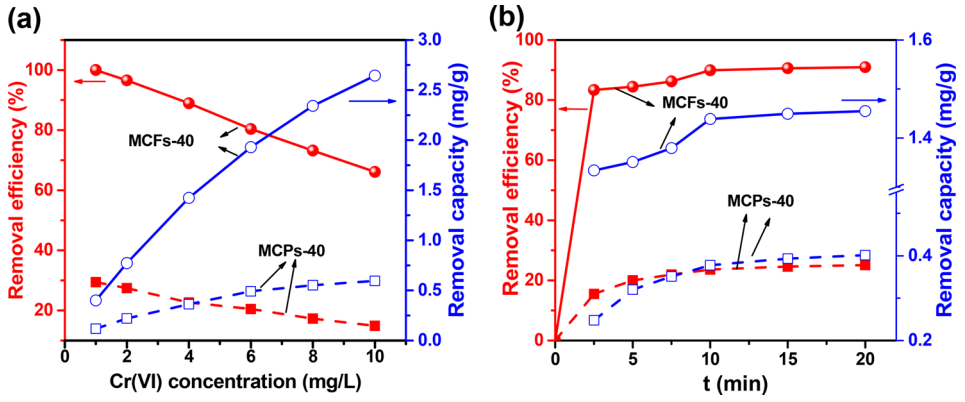

Figure 6. Effect of Cr (VI) concentration (a) and contact time (b) on Cr(VI) removal efficiency and capacity for the synthesized MCFs-40 and MCPs-40. The condition were 2.5 g/L adsorbents, pH 7, and ultrasonic treatment for 10 min.

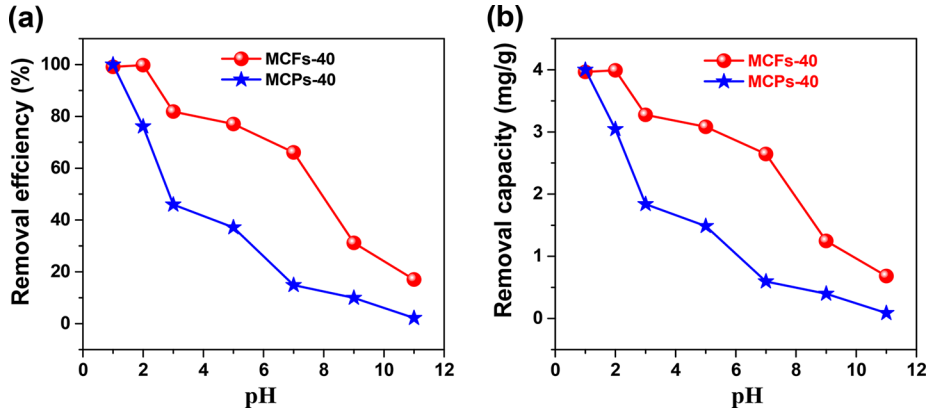

Figure 7. Effect of pH on Cr(VI) removal efficiency (a) and Cr(VI) removal capacity (b) for the synthesized MCFs-40 and MCPs-40. The experiment conditions were 2.5 g/L adsorbents, Cr(VI) solution (10 mg/L), and ultrasonic treatment for 10 min.

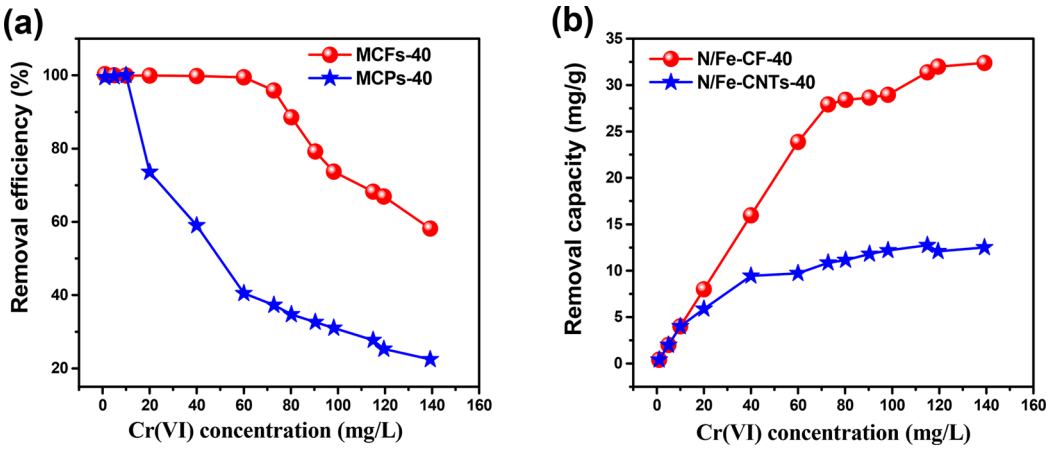

Figure 8. Effect of Cr(VI) on Cr(VI) removal efficiency (a) and Cr(VI) removal capacity (b) for the synthesized MCFs-40 and MCPs-40. The experiment conditions were 2.5 g/L adsorbents, Cr(VI) solution (10 mg/L) with pH 1, and ultrasonic treatment for 10 min.

and the removal efficiency and capacity of MCFs-40 were enhanced only about 13.3% and 9.0%, respectively. This observation can be concluded that the active sites might be gradually covered by the adsorbed metal ions and thus caused adsorption saturation.[57] It is worth noting that the efficiency and capacity of MCFs-40 were still about 3 times higher than those of MCPs-40.

The pH value is one of the most important parameters affecting the Cr(VI) removal performance. It is observed that both higher Cr(VI) removal efficiency and capacity were obtained in a low pH solution (Figure 7). Cr(VI) was totally removed by 2.5 g/L MCFs-40 and MCPs-40 samples in 20 mL of Cr(VI) solution (10 mg/L) with a Cr(VI) solution pH of 1.0. The Cr(VI) removal performance decreased gradually with the increase of the pH value, due to the weakened oxidizability of Cr(VI) in acidic conditions, which improved the redox reaction with the iron particles or carbon atoms at the edges.[55,87] The Cr(VI) ions were in the form of CrO_4^{2-}, $HCrO_4^-$, H_2CrO_4, $Cr_2O_7^{2-}$, and $HCr_2O_7^-$, relying on the solution pH value and total chromate concentration.[88] The five

DOI: 10.1021/acs.iecr.7b02835
Ind. Eng. Chem. Res. 2017, 56, 10689−10701

Cr(VI) ion species were obtained by the following equilibrium reactions:[69,87−89]

$$CrO_4^- + H^+ \rightleftharpoons HCrO_4^- \quad (5)$$

$$HCrO_4^- + H^+ \rightleftharpoons H_2CrO_4 \quad (6)$$

$$2HCrO_4^- \rightleftharpoons Cr_2O_7^{2-} + H_2O \quad (7)$$

$$Cr_2O_7^{2-} + H^+ \rightleftharpoons HCr_2O_7^- \quad (8)$$

$HCrO_4^-$, $Cr_2O_7^{2-}$, and $HCr_2O_7^-$ were the main species of Cr(VI) in the condition of pH <6.8, while CrO_4^{2-} was the dominant stable species in the condition of pH >6.8.[46,51,53] Thus, Cr(VI) was reduced to Cr(III) by α-Fe, γ-Fe, and FeO on the surface of adsorbents more easily in acid condition than that in neutral condition, due to the high oxidability of $HCrO_4^-$ and $Cr_2O_7^{2-}$.[46,51,53] Furthermore, the fast protonation of the active sites X−OH (X = Fe, C) on the material surfaces led to the formation of $X-OH_2^+$ groups, thereby resulting in the adsorption of $HCrO_4^-$ and $Cr_2O_7^{2-}$ at even lower pH solutions ($1 < pH < 4$).[67]

For the acid circumstance (pH 1), the effects of initial Cr(VI) concentration with two kinds of adsorbents were investigated. A total of 20 mL of Cr(VI) solution with different Cr(VI) concentrations (1−140 mg/L) was used as pollution water (Figure 8). In this study, the removal efficiency of MCFs-40 samples was maintained at about 100% when the Cr(VI) concentration increased from 1 to 70 mg/L, and then the removal efficiency decreased sharply to about 60% in 140 mg/L Cr(VI). This performance was much better than that of MCPs-40. The removal efficiency of MCPs-40 decreased dramatically from 100 to 40% with increasing the Cr(VI) concentration from 10 to 60 mg/L. The removal capacity of MCPs-40 was 32.5 mg/g at 140 mg/L Cr(VI) solution, while the removal capacity of MCPs-40 was about 12.5 mg/g only. It was demonstrated that the removal performance of MCFs-40 and MCPs-40 adsorbents was very sensitive to the Cr(VI) concentration with pH value at 1, but the adsorptive performance of MCPs-40 was much lower than that of MCFs-40.

3.5. Adsorption Kinetic and Isotherms Study. The sorption type (physical or chemical sorption) of metal ions over MCFs-40 and MCPs-40 nanoadsorbents was investigated (Figure S3). The correlation coefficient (R^2) of the models was used to evaluate the suitability of different models.[55,87] The higher values of R^2 in the pseudo second order kinetics were obtained for Cr(VI) ions sorption onto MCPs (0.98) and MCFs (0.99) than those in pseudo first order kinetics (0.92 and 0.72 for MCPs and MCFs, respectively), indicating that the adsorptions of Cr(VI) ions onto MCPs and MCFs were more suitable to be described by the pseudo second order model. These results demonstrated that the chemical sorption involving valence forces through exchange or sharing of electrons between adsorbents and adsorbates was conformed in this work.

The Cr(VI) removal performance over those two kinds of adsorbents at different time intervals are shown in Figure S4. Higher the adsorption rate constants also were observed over fibrillar sample (2.733 g/(mg min)) than the particulate sample (2.200 g/(mg min); Table S6). The Cr(VI) removals for the MCPs-40 and MCFs-40 nanoadsorbents in neutral and acid solutions were fitted with the Langmuir and Freundlich models very well (Figure S5), and the constants n of MCPs-40 (in acid solution) and MCFs-40 (in neutral and acid solution) were over 1, indicating a favorable condition for adsorption (Table S6). The calculated maximum Cr(VI) removal capacities (q_{max}) of MCFs-40 based on the Langmuir model were about 7.03 and 43.18 mg/g in neutral and acid solution, respectively, much higher than those of MCPs-40 adsorbents (1.10 and 15.89 in neutral and acid solution, respectively), demonstrating that the fibrillar samples displayed much higher efficiency than the particulate samples in Cr(VI) removal. The Cr(VI) removal efficiencies of various adsorbents are summarized in Table 1

Table 1. Comparison of Cr(VI) Removal Capacity Using Fibrillar and Particulate Magnetic Carbons with Other Adsorbents

adsorbent	pH	equilibrium time (min)	specific surface area (m^2/g)	q_{max} (mg/g)	ref
granular activated carbon	3.0	3600	950.0	2.21	93
carbon slurry	2.0	70	388.0	15.24	94
aminated polyacrylonitrile/ ferrous fibers	2.5	120		20.7	90
polyacrylonitrile/ ferrous chloride fibers	5	125	13.8	5.04	95
magnetic carbon fabrics	2.0	10	295.9	4.20	51
polyaniline coated carbon fibers	1.0	15	1622.4	18.10	96
magnetic nanoparticles	2.5	120	86.6	20.16	97
surface modified magnetic nanoparticles	2.0	5	208.0	31.55	91
magnetic Fe_3O_4 nanoparticles	4.0	120	190.0	35.46	98
active carbon fibers	3.0	600	1690.0	20.49	61
pitch-based activated carbon fibers	3.0	1440	1914.0	24.90	92
magnetic carbon particles (MCPs)	1.0	10	32.6	15.89	this work
magnetic carbon fibers (MCFs)	1.0	10	124.7	43.18	this work

with the values of the magnetic carbon particles and magnetic carbon fibers in this work, demonstrating that the Cr(VI) removal capacity of the magnetic carbon fiber in this work was comparative to other similar fiber or particle materials, such as PAN/ferrous chloride fibers,[90] surface modified magnetic nanoparticles,[91] pitch-based activated carbon fibers,[92] and so on.

3.6. Reusability of the Adsorbents in the Cr(VI) Removal. The reusability of adsorbents is the key parameter for practical applications. In this study, MCFs-40 and MCPs-40 were selected to conduct the stability investigation. After each recycle, the adsorbents were washed by 0.1 M NaOH solution and deionized water to regenerate the adsorbents. As shown in Figure 9a, no significant change of the performance over MCFs-40 and MCPs-40 was observed after 5 recycles, demonstrating the acceptable stability of these two adsorbents in the Cr(VI) removal in the neutral condition. The adsorbent can be reused in the neutral solution as the redox reaction cannot consume the magnetic nanoparticles so fast and in this process, since the adsorption behavior played a dominant role. The redox reaction also occurred, since the removal perform-

DOI: 10.1021/acs.iecr.7b02835
Ind. Eng. Chem. Res. 2017, 56, 10689−10701

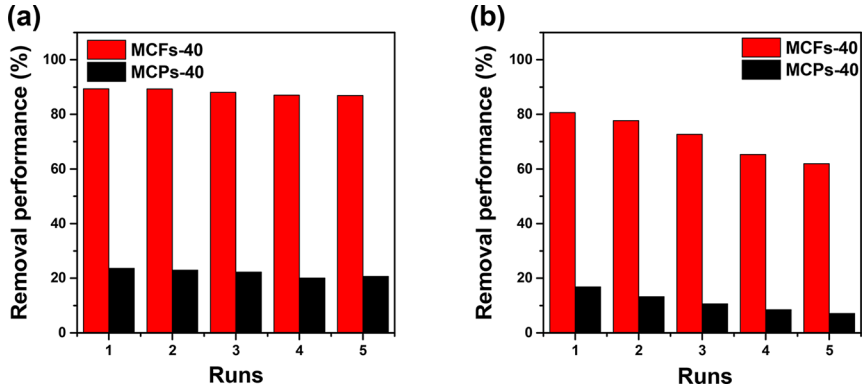

Figure 9. Stability of the fibrillar (MCFs-40) and particulate (MCPs-40) adsorbents in the Cr(VI) removal. The experiment conditions were (a) 2.5 g/L adsorbents, 4 mg/L Cr(VI), pH 7, and ultrasonic treatment for 10 min; (b) 2.5 g/L adsorbents, 4 mg/L Cr(VI), pH 7, and ultrasonic treatment for 10 min, 2 mg/L $Ni(NO_3)_2{\cdot}6H_2O$, 2 mg/L $CuCl_2$, 2 mg/L $Fe_2(SO_4)_3$, and 2 mg/L $Zn_3(PO_4)_2$.

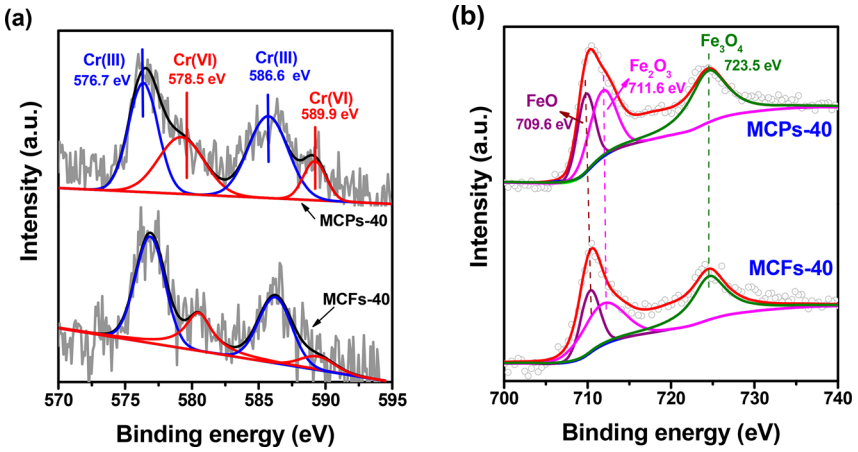

Figure 10. (a) Cr 2p and (b) Fe 2p XPS spectra of the fibrillar and particulate carbon adsorbents after Cr-removal.

ance was decreased slightly after each test. In addition, we cannot test the stability in the acid solution, because the magnetic nanoparticles would be consumed intermedium, reacting with not only Cr(VI) ions but also H^+ ions in the system. This would destroy the structure of adsorbents, and it would lose the most activity. In order to the evaluate the recovery of the chromium in the real wastewater, which usually contains diverse anions and cations, we added 2 mg/L $Ni(NO_3)_2{\cdot}6H_2O$, 2 mg/L $CuCl_2$, 2 mg/L $Fe_2(SO_4)_3$, and 2 mg/L $Zn_3(PO_4)_2$ into the Cr(VI) solution (Figure 9b). The recycle test results showed that the adoption ability of both adsorbents declined, due to the saturation of the active site covered by other ions. Nevertheless, the MCFs-40 still displayed a comparative stability for the Cr(VI) removal in the present condition.

3.7. Cr(VI) Removal Mechanism. In order to investigate the mechanism of Cr(VI) removal over MCFs-40 and MCPs-40 samples, the chemical compositions of used sample surfaces were measured by XPS (Figures 10 and S6 and Table S7). When the MCFs-40 and MCPs-40 adsorbents were treated in neutral Cr(VI) solutions, the peaks of Cr_{2p} were observed in full range XPS spectra of both samples, demonstrating that Cr(VI) ions were adsorbed on the surface of both adsorbents. The deconvolution of Cr_{2p} peaks was also conducted. The Cr(III) peaks (576.7 and 586.6 eV) and Cr(VI) peaks (578.5 and 589.9 eV) were obtained (Figure 10a).[86] What's more, the contents of Cr(III) were much higher than that of Cr(VI) after treated in neutral Cr(VI) solutions, indicating that the produced Cr(III) was the main species of Cr adsorbed over both samples (Table 2).[57] Therefore, the reduction of Cr(VI) to Cr(III) played a significant role on the Cr(VI) removal in MCFs-40 and MCPs-40 nanoadsorbents. Furthermore, no Fe^0 particles (706.9 eV) were found in the Fe_{2p} XPS spectra of MCFs-40 and MCPs-40 after Cr(VI) removal, indicating that Fe^0 nanoparticles in the fresh samples totally reacted with Cr(VI) ions to produce Fe^{3+} and Cr(III) ions during this process (Figure 10b).[51,69] In addition, we believed that the Cr(VI) ions had strong oxidizability to oxidize the magnetic carbons. In this study, the carbon shell of MCPs-40 may be oxidized, and the structure was collapsed after treatment; hence, more Fe components were exposed. Meanwhile, it was hard to change the MCFs-40 structure due to the uniform fiber morphology. Therefore, the slightly higher Fe component of MCPs (0.8 atmoic %) after treatment was observed.

Table 2. Quantitative XPS Analysis of Cr_{2p} and Fe_{2p} on the Fresh and Treated Samples

	Cr_{2p} (%).		Fe_{2p} (%).		
samples	Cr(III)	Cr(VI)	FeO	Fe_2O_3	Fe_3O_4
treated MCFs-40	72.4	27.6	12.8	31.3	55.9
treated MCPs-40	65.1	34.9	15.8	32.9	51.3

DOI: 10.1021/acs.iecr.7b02835
Ind. Eng. Chem. Res. 2017, 56, 10689−10701

Cr(VI) removal combines with adsorption and redox reaction in the current study. For the redox reaction between the carbon adsorbents and Cr(VI) ions, our previous work has revealed that the Fe^0, Fe^{2+} nanoparticles and carbon atoms at edges would react with Cr(VI) ion to produce Cr(III) ions.[58,99] Oxygen containing groups on the carbon surface will be generated during the redox process. Figure 11 shows the O_{1s}

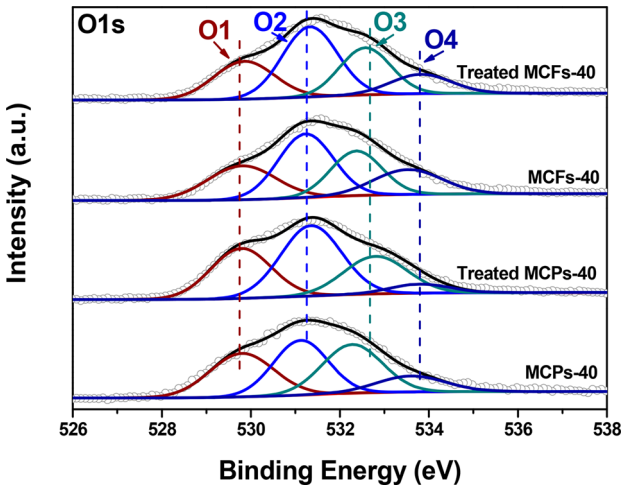

Figure 11. O_{1s} XPS spectra of the fresh and after treated magnetic carbons.

XPS spectra of the fresh and the treated MCFs-40. Four peaks centered at 530.7, 531.7, 532.8, and 533.6 eV were deconvoluted, corresponding to quinonic C═O (O1), ketonic C═O (O2), ether-like C−O−C (O3), and hydroxyl C−OH (O4) groups, respectively.[100] As seen that after treatment from Table 3, the content of oxygen containing groups, for instance

Table 3. Quantitative XPS Analysis of O_{1s} on the Fresh and Treated Samples[a]

		O_{1s} (at. %)			
samples	O (at. %).	O1	O2	O3	O4
MCFs-40	8.8	2.1	3.1	2.1	1.5
MCPs-40	6.3	1.8	1.9	1.9	0.7
treated MCFs-40	8.6	2.5	4.2	2.6	1.3
treated MCPs-40	10.6	2.6	3.5	2.0	0.5

[a]O1: quinonic C═O; O2: ketonic C═O; O3: etherlike C−O−C; O4: hydroxyl C−OH.

quinonic C═O and ketonic C═O, were greatly increased, similar to our previous work.[58] This result demonstrated that the carbons surface can be oxidized by the Cr(VI) ions with more oxygen species and Cr(III) ions produced,[99] which could be abbreviated by eq 9:

$$HCrO_4^-(aq) + \text{carbons}(s) \rightarrow Cr^{3+}(aq) + \text{carbons} - O(s) \quad (9)$$

The magnetization results of MCPs-40 and MCFs-40 (Figure S7) showed that the saturated magnetization (M_s) values of fresh MCPs-40 and MCFs-40 nanoadsorbents were 40.22 and 16.29 emu/g, respectively. The coercive force (H_c) values of fresh MCPs-40 and MCFs-40 were 97.84 O_e and 375.19 O_e, respectively. The MCPs-40 adsorbents, showing low adsorptive capacity in neutral and acid solution, had higher M_s than that of MCFs-40, demonstrating that the magnetic properties did not play a dominating role in the Cr(VI) removal. Furthermore, the decreasing of the M_s value was observed after the Cr(VI) removal. Compared with the fresh adsorbents, the M_s value of the treated samples (25.55 and 15.80 emu/g for MCPs-40 and MCFs-40, respectively) did not change significantly in neutral condition (pH 7.0) but decreased dramatically after being treated in acid condition (pH 1.0; 0.82 and 7.76 emu/g for MCPs-40 and MCFs-40, respectively). Both adsorbents showed higher adsorptive capacity in acid solutions than that in neutral solutions, Figure 7, due to the strong oxidability of $HCrO_4^-$ and $Cr_2O_7^{2-}$ in acid condition. The lower M_s value of the treated samples in acid solution than that in neutral solution may be caused by the consumption of Fe^0 and Fe^{2+} species on the surface of samples in acid solutions. The thermogravimetric analysis (TGA) results of the fresh and treated samples (Figure S8) showed that the final weight loss of the MCPs-40 and MCFs-40 treated with acid Cr(VI) solution was higher than those treated with neutral solutions, indicating that fewer metal species (Fe or Cr) were remained in the samples. From the XPS data (Table S1) the Fe element exposed on the surface of these two kinds of adsorbents was too low, meaning that the magnetic particles were consumed not too much after treatment. Meanwhile, because the Cr(VI) and Cr(III) would be adsorbed onto the adsorbents, the Fe and Fe^{2+} would be consumed after the treatment. Therefore, it was reasonable that the weight loss of MCPs-40 could not be changed too much before and after the treatment. It was said that, when the adsorbents were treated at acid condition, more Fe^0 and Fe^{2+} nanoparticles reacted with Cr(VI) ions than those treated in neutral solution, due to the involvement of more H^+ ions, which enhanced the oxidizability of Cr(VI) ions.[51] The higher final weight loss of MCPs-40 (pH at 7) than that of fresh MCPs-40, Figure S8a, was probably due to the adsorbed Cr(VI) and Cr(III) ions on the surface (Figure 10), since the weight of the Cr complex was heavier than the Fe^0 particles. Meanwhile, the similar value of R ratios of MCFs-40 and MCPs-40 in Raman (Figure 3) revealed that similar defects of graphite were obtained in both samples and caused the formation of functional groups on the carbon. Herein the reduction capacities of carbon for Cr(VI) removal were similar in MCFs-40 and MCPs-40 samples. The higher specific surface area of fresh MCFs-40 than that of fresh MCPs-40 adsorbents (Figure 4 and Table 1) indicates more adsorptive sites on MCFs-40 for metal (Cr(VI) and Cr(III) ions) sorption on the carbon surface. Thus, the Cr(VI) adsorptive capacities of MCFs-40 were higher than that of MCPs-40. The Cr(VI) removal mechanisms by MCFs and MCPs are summarized in Scheme 1.

4. CONCLUSIONS

In summary, magnetic carbons with different morphologies, fibrillar (MCFs) and particulate (MCPs), were synthesized by using electrospinning technology and annealing method. These two kinds of magnetic carbons were applied and displayed high efficiency for Cr(VI) removal. The sorption pseudo-second order kinetics over the magnetic carbons revealed that the type of adsorption was chemisorption. The Cr(VI) removal efficiency over MCFs-40 was about three times higher than that of MCPs-40 in neutral solution, which was attributed to higher specific surface area of MCFs-40. Specially, the Cr(VI) (20 mL, 1.0 mg/L, pH 7) was totally removed by 2.5 g/L MCFs-40 in 10 min, while only 29.3% Cr(VI) was removed by

DOI: 10.1021/acs.iecr.7b02835
Ind. Eng. Chem. Res. 2017, 56, 10689−10701

Scheme 1. Cr(VI) Removal Mechanism over Fibrillar and Particulate Magnetic Carbon Adsorbents

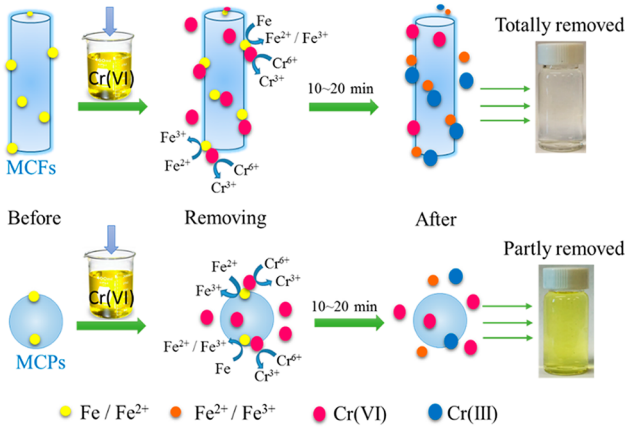

2.5 g/L MCPs. In the acid solutions, the enhanced Cr(VI) removal in both of them were observed, ascribed to the involved H^+ ions and the faster protonation of the surface-active sites. When the pH of solution was 1, the calculated maximum Cr(VI) removal capacities of MCPs-40 and MCFs-40 were 15.89 and 43.17 mg/g, respectively. The M_s and XPS results demonstrated that the reduction between Cr(VI) and Fe^0 nanoparticles or carbon atoms occurred. The Cr(VI) and Cr(III) were found on the treated MCPs-40 and MCFs-40, indicating that the Cr(VI) and the produced Cr(III) ions were adsorbed on the samples surfaces.

■ ASSOCIATED CONTENT

Supporting Information

The Supporting Information is available free of charge on the ACS Publications website at DOI: 10.1021/acs.iecr.7b02835.

Additional characterization, adsorption kinetic study, and more discussion. (PDF)

■ AUTHOR INFORMATION

Corresponding Authors

*E-mail: meyhcao@scut.edu.cn. Fax/Phone: +86 020 87114916.

*E-mail: zguo10@utk.edu. Phone: (865) 974-2933.

ORCID

Yonghai Cao: 0000-0003-0035-6253

Zhanhu Guo: 0000-0003-0134-0210

Notes

The authors declare no competing financial interest.

■ ACKNOWLEDGMENTS

This project is financially supported by the start-up fund of University of Tennessee, National Natural Science Foundation of China (Nos. 21503082 and 51573063), Guangdong Provincial National Science Foundation (Nos. 2014A030310447), and Guangdong Science and Technology Planning Project (No. 2014B010104004).

■ REFERENCES

(1) Gupta, V. K.; Kumar, R.; Nayak, A.; Saleh, T. A.; Barakat, M. Adsorptive removal of dyes from aqueous solution onto carbon nanotubes: a review. *Adv. Colloid Interface Sci.* **2013**, *193*, 24−34.

(2) Saleh, T. A.; Gupta, V. K. Processing methods, characteristics and adsorption behavior of tire derived carbons: a review. *Adv. Colloid Interface Sci.* **2014**, *211*, 93−101.

(3) Gupta, V. K.; Nayak, A.; Agarwal, S. Bioadsorbents for remediation of heavy metals: Current status and their future prospects. *Environ. Eng. Res.* **2015**, *20*, 1−18.

(4) Gupta, V. K.; Saleh, T. A. Sorption of pollutants by porous carbon, carbon nanotubes and fullerene-An overview. *Environ. Sci. Pollut. Res.* **2013**, *20*, 2828−2843.

(5) Gupta, V. K.; Ali, I.; Saleh, T. A.; Nayak, A.; Agarwal, S. Chemical treatment technologies for waste-water recycling—an overview. *RSC Adv.* **2012**, *2*, 6380−6388.

(6) Gupta, V. K.; Imran, A. Adsorbents for water treatment: development of low-cost alternatives to carbon. *Encyclopedia of Surface and Colloid Science*; 2004 Update Supplement; Marcel Dekker, Inc.: New York, 2004.

(7) Gupta, V. K.; Nayak, A. Cadmium removal and recovery from aqueous solutions by novel adsorbents prepared from orange peel and Fe_2O_3 nanoparticles. *Chem. Eng. J.* **2012**, *180*, 81−90.

(8) Saleh, T. A.; Gupta, V. K. Column with CNT/magnesium oxide composite for lead(II) removal from water. *Environ. Sci. Pollut. Res.* **2012**, *19*, 1224−1228.

(9) Ahmaruzzaman, M.; Gupta, V. K. Rice husk and its ash as low-cost adsorbents in water and wastewater treatment. *Ind. Eng. Chem. Res.* **2011**, *50*, 13589−13613.

(10) Mittal, A.; Mittal, J.; Malviya, A.; Gupta, V. K. Removal and recovery of Chrysoidine Y from aqueous solutions by waste materials. *J. Colloid Interface Sci.* **2010**, *344*, 497−507.

(11) Mittal, A.; Mittal, J.; Malviya, A.; Kaur, D.; Gupta, V. K. Decoloration treatment of a hazardous triarylmethane dye, Light Green SF (Yellowish) by waste material adsorbents. *J. Colloid Interface Sci.* **2010**, *342*, 518−527.

(12) Karthikeyan, S.; Gupta, V.; Boopathy, R.; Titus, A.; Sekaran, G. A new approach for the degradation of high concentration of aromatic amine by heterocatalytic Fenton oxidation: kinetic and spectroscopic studies. *J. Mol. Liq.* **2012**, *173*, 153−163.

(13) Saravanan, R.; Gracia, F.; Khan, M. M.; Poornima, V.; Gupta, V. K.; Narayanan, V.; Stephen, A. ZnO/CdO nanocomposites for textile effluent degradation and electrochemical detection. *J. Mol. Liq.* **2015**, *209*, 374−380.

(14) Saravanan, R.; Gupta, V. K.; Narayanan, V.; Stephen, A. Comparative study on photocatalytic activity of ZnO prepared by different methods. *J. Mol. Liq.* **2013**, *181*, 133−141.

(15) Saravanan, R.; Thirumal, E.; Gupta, V.; Narayanan, V.; Stephen, A. The photocatalytic activity of ZnO prepared by simple thermal decomposition method at various temperatures. *J. Mol. Liq.* **2013**, *177*, 394−401.

(16) Saravanan, R.; Gupta, V. K.; Mosquera, E.; Gracia, F.; Narayanan, V.; Stephen, A. Visible light induced degradation of methyl orange using β-Ag 0.333 V_2O_5 nanorod catalysts by facile thermal decomposition method. *J. Saudi Chem. Soc.* **2015**, *19*, 521−527.

(17) Gupta, V. K.; Jain, R.; Mittal, A.; Saleh, T. A.; Nayak, A.; Agarwal, S.; Sikarwar, S. Photo-catalytic degradation of toxic dye amaranth on TiO_2/UV in aqueous suspensions. *Mater. Sci. Eng., C* **2012**, *32*, 12−17.

(18) Gupta, V. K.; Jain, R.; Nayak, A.; Agarwal, S.; Shrivastava, M. Removal of the hazardous dye—Tartrazine by photodegradation on titanium dioxide surface. *Mater. Sci. Eng., C* **2011**, *31*, 1062−1067.

(19) Saravanan, R.; Karthikeyan, N.; Gupta, V.; Thirumal, E.; Thangadurai, P.; Narayanan, V.; Stephen, A. ZnO/Ag nanocomposite: an efficient catalyst for degradation studies of textile effluents under visible light. *Mater. Sci. Eng., C* **2013**, *33*, 2235−2244.

(20) Gupta, V. K.; Mittal, A.; Jhare, D.; Mittal, J. Batch and bulk removal of hazardous colouring agent Rose Bengal by adsorption techniques using bottom ash as adsorbent. *RSC Adv.* **2012**, *2*, 8381−8389.

(21) Saravanan, R.; Khan, M. M.; Gupta, V. K.; Mosquera, E.; Gracia, F.; Narayanan, V.; Stephen, A. ZnO/Ag/Mn2O3 nanocomposite for

visible light-induced industrial textile effluent degradation, uric acid and ascorbic acid sensing and antimicrobial activity. *RSC Adv.* **2015**, *5*, 34645−34651.
(22) Rajendran, S.; Khan, M. M.; Gracia, F.; Qin, J.; Gupta, V. K.; Arumainathan, S. Ce^{3+}-ion-induced visible-light photocatalytic degradation and electrochemical activity of ZnO/CeO_2 nanocomposite. *Sci. Rep.* **2016**, *6*, 31641.
(23) Jain, A.; Gupta, V.; Bhatnagar, A.; Suhas. A comparative study of adsorbents prepared from industrial wastes for removal of dyes. *Sep. Sci. Technol.* **2003**, *38*, 463−481.
(24) Gupta, V. K.; Srivastava, S. K.; Mohan, D.; Sharma, S. Design parameters for fixed bed reactors of activated carbon developed from fertilizer waste for the removal of some heavy metal ions. *Waste Manage.* **1998**, *17*, 517−522.
(25) Saravanan, R.; Sacari, E.; Gracia, F.; Khan, M. M.; Mosquera, E.; Gupta, V. K. Conducting PANI stimulated ZnO system for visible light photocatalytic degradation of coloured dyes. *J. Mol. Liq.* **2016**, *221*, 1029−1033.
(26) Saravanan, R.; Prakash, T.; Gupta, V.; Stephen, A. Tailoring the electrical and dielectric properties of ZnO nanorods by substitution. *J. Mol. Liq.* **2014**, *193*, 160−165.
(27) Saravanan, R.; Khan, M. M.; Gupta, V. K.; Mosquera, E.; Gracia, F.; Narayanan, V.; Stephen, A. ZnO/Ag/CdO nanocomposite for visible light-induced photocatalytic degradation of industrial textile effluents. *J. Colloid Interface Sci.* **2015**, *452*, 126−133.
(28) Saravanan, R.; Karthikeyan, S.; Gupta, V.; Sekaran, G.; Narayanan, V.; Stephen, A. Enhanced photocatalytic activity of ZnO/CuO nanocomposite for the degradation of textile dye on visible light illumination. *Mater. Sci. Eng., C* **2013**, *33*, 91−98.
(29) Saravanan, R.; Joicy, S.; Gupta, V.; Narayanan, V.; Stephen, A. Visible light induced degradation of methylene blue using CeO_2/V_2O_5 and CeO_2/CuO catalysts. *Mater. Sci. Eng., C* **2013**, *33*, 4725−4731.
(30) Saravanan, R.; Gupta, V.; Prakash, T.; Narayanan, V.; Stephen, A. Synthesis, characterization and photocatalytic activity of novel Hg doped ZnO nanorods prepared by thermal decomposition method. *J. Mol. Liq.* **2013**, *178*, 88−93.
(31) Saravanan, R.; Gupta, V.; Narayanan, V.; Stephen, A. Visible light degradation of textile effluent using novel catalyst ZnO/γ-Mn_2O_3. *J. Taiwan Inst. Chem. Eng.* **2014**, *45*, 1910−1917.
(32) Saravanan, R.; Gupta, V.; Mosquera, E.; Gracia, F. Preparation and characterization of V_2O_5/ZnO nanocomposite system for photocatalytic application. *J. Mol. Liq.* **2014**, *198*, 409−412.
(33) Saleh, T. A.; Gupta, V. K. Synthesis and characterization of alumina nano-particles polyamide membrane with enhanced flux rejection performance. *Sep. Purif. Technol.* **2012**, *89*, 245−251.
(34) Saleh, T. A.; Gupta, V. K. Photo-catalyzed degradation of hazardous dye methyl orange by use of a composite catalyst consisting of multi-walled carbon nanotubes and titanium dioxide. *J. Colloid Interface Sci.* **2012**, *371*, 101−106.
(35) Saleh, T. A.; Gupta, V. K. Functionalization of tungsten oxide into MWCNT and its application for sunlight-induced degradation of rhodamine B. *J. Colloid Interface Sci.* **2011**, *362* (2), 337−344.
(36) Mohammadi, N.; Khani, H.; Gupta, V. K.; Amereh, E.; Agarwal, S. Adsorption process of methyl orange dye onto mesoporous carbon material−kinetic and thermodynamic studies. *J. Colloid Interface Sci.* **2011**, *362*, 457−462.
(37) Mittal, A.; Mittal, J.; Malviya, A.; Gupta, V. K. Adsorptive removal of hazardous anionic dye "Congo red" from wastewater using waste materials and recovery by desorption. *J. Colloid Interface Sci.* **2009**, *340*, 16−26.
(38) Mittal, A.; Kaur, D.; Malviya, A.; Mittal, J.; Gupta, V. K. Adsorption studies on the removal of coloring agent phenol red from wastewater using waste materials as adsorbents. *J. Colloid Interface Sci.* **2009**, *337*, 345−354.
(39) Khani, H.; Rofouei, M. K.; Arab, P.; Gupta, V. K.; Vafaei, Z. Multi-walled carbon nanotubes-ionic liquid-carbon paste electrode as a super selectivity sensor: Application to potentiometric monitoring of mercury ion(II). *J. Hazard. Mater.* **2010**, *183*, 402−409.
(40) Gupta, V. K.; Agarwal, S.; Saleh, T. A. Synthesis and characterization of alumina-coated carbon nanotubes and their application for lead removal. *J. Hazard. Mater.* **2011**, *185*, 17−23.
(41) Devaraj, M.; Saravanan, R.; Deivasigamani, R.; Gupta, V. K.; Gracia, F.; Jayadevan, S. Fabrication of novel shape Cu and Cu/Cu_2O nanoparticles modified electrode for the determination of dopamine and paracetamol. *J. Mol. Liq.* **2016**, *221*, 930−941.
(42) Sun, Z.; Zhang, L.; Dang, F.; Liu, Y.; Fei, Z.; Shao, Q.; Lin, H.; Guo, J.; Xiang, L.; Yerra, N.; Guo, Z. Experimental and simulation-based understanding of morphology controlled barium titanate nanoparticles under co-adsorption of surfactants. *CrystEngComm* **2017**, *19*, 3288−3298.
(43) Zhang, L.; Yu, W.; Han, C.; Guo, J.; Zhang, Q.; Xie, H.; Shao, Q.; Sun, Z.; Guo, Z. Large Scaled Synthesis of Heterostructured Electrospun TiO_2/SnO_2 Nanofibers with an Enhanced Photocatalytic Activity. *J. Electrochem. Soc.* **2017**, *164*, H651−H656.
(44) Zou, Y.; Wang, X.; Khan, A.; Wang, P.; Liu, Y.; Alsaedi, A.; Hayat, T.; Wang, X. Environmental Remediation and Application of Nanoscale Zero-Valent Iron and Its Composites for the Removal of Heavy Metal Ions: A Review. *Environ. Sci. Technol.* **2016**, *50*, 7290−7304.
(45) Wang, H.; Na, C. Binder-Free Carbon Nanotube Electrode for Electrochemical Removal of Chromium. *ACS Appl. Mater. Interfaces* **2014**, *6*, 20309−20316.
(46) Zhang, D.; Wei, S. Y.; Kaila, C.; Su, X.; Wu, J.; Karki, A. B.; Young, D. P.; Guo, Z. H. Carbon-stabilized iron nanoparticles for environmental remediation. *Nanoscale* **2010**, *2*, 917−919.
(47) Yusof, A. M.; Malek, N. A. N. N. Removal of Cr(VI) and As(V) from aqueous solutions by HDTMA-modified zeolite Y. *J. Hazard. Mater.* **2009**, *162*, 1019−1024.
(48) Kratochvil, D.; Pimentel, P.; Volesky, B. Removal of trivalent and hexavalent chromium by seaweed biosorbent. *Environ. Sci. Technol.* **1998**, *32*, 2693−2698.
(49) Szabó, A.; Gournis, D.; Karakassides, M. A.; Petridis, D. Clay−Aminopropylsiloxane Compositions. *Chem. Mater.* **1998**, *10*, 639−645.
(50) Tamai, H.; Kakii, T.; Hirota, Y.; Kumamoto, T.; Yasuda, H. Synthesis of Extremely Large Mesoporous Activated Carbon and Its Unique Adsorption for Giant Molecules. *Chem. Mater.* **1996**, *8*, 454−462.
(51) Zhu, J. H.; Gu, H. B.; Guo, J.; Chen, M. J.; Wei, H. G.; Luo, Z. P.; Colorado, H. A.; Yerra, N.; Ding, D.; Ho, T. C.; Haldolaarachchige, N.; Hopper, J.; Young, D. P.; Guo, Z. H.; Wei, S. Y. Mesoporous magnetic carbon nanocomposite fabrics for highly efficient Cr(VI) removal. *J. Mater. Chem. A* **2014**, *2*, 2256−2265.
(52) Shashkova, I. L.; Rat'ko, A. I.; Kitikova, N. V. Removal of heavy metal ions from aqueous solutions by alkaline-earth metal phosphates. *Colloids Surf., A* **1999**, *160*, 207−215.
(53) Qiu, B.; Gu, H.; Yan, X.; Guo, J.; Wang, Y.; Sun, D.; Wang, Q.; Khan, M.; Zhang, X.; Weeks, B. L.; Young, D. P.; Guo, Z.; Wei, S. Cellulose derived magnetic mesoporous carbon nanocomposites with enhanced hexavalent chromium removal. *J. Mater. Chem. A* **2014**, *2*, 17454−17462.
(54) Liu, X.; Pan, L.; Lv, T.; Zhu, G.; Sun, Z.; Sun, C. Microwave-assisted synthesis of CdS-reduced graphene oxide composites for photocatalytic reduction of Cr(VI). *Chem. Commun.* **2011**, *47*, 11984−11986.
(55) Zhu, J. H.; Wei, S. Y.; Chen, M. J.; Gu, H. B.; Rapole, S. B.; Pallavkar, S.; Ho, T. C.; Hopper, J.; Guo, Z. H. Magnetic nanocomposites for environmental remediation. *Adv. Powder Technol.* **2013**, *24*, 459−467.
(56) Anderson, R. A. Chromium as an Essential Nutrient for Humans. *Regul. Toxicol. Pharmacol.* **1997**, *26*, S35−S41.
(57) Cao, Y.; Huang, J.; Li, Y.; Qiu, S.; Liu, J.; Khasanov, A.; Khan, M. A.; Young, D. P.; Peng, F.; Cao, D.; Peng, X.; Hong, K.; Guo, Z. One-pot melamine derived nitrogen doped magnetic carbon nano-adsorbents with enhanced chromium removal. *Carbon* **2016**, *109*, 640−649.
(58) Cao, Y.; Huang, J.; Peng, X.; Cao, D.; Galaska, A.; Qiu, S.; Liu, J.; Khan, M. A.; Young, D. P.; Ryu, J. E.; Feng, H.; Yerra, N.; Guo, Z.

DOI: 10.1021/acs.iecr.7b02835
Ind. Eng. Chem. Res. 2017, 56, 10689−10701

Poly(vinylidene fluoride) derived fluorine-doped magnetic carbon nanoadsorbents for enhanced chromium removal. *Carbon* **2017**, *115*, 503−514.
(59) Zhu, J. H.; Wei, S. Y.; Gu, H. B.; Rapole, S. B.; Wang, Q.; Luo, Z. P.; Haldolaarachchige, N.; Young, D. P.; Guo, Z. H. One-Pot Synthesis of Magnetic Graphene Nanocomposites Decorated with Core@Double-shell Nanoparticles for Fast Chromium Removal. *Environ. Sci. Technol.* **2012**, *46*, 977−985.
(60) Yan, F.-F.; Wu, C.; Cheng, Y.-Y.; He, Y.-R.; Li, W.-W.; Yu, H.-Q. Carbon nanotubes promote Cr(VI) reduction by alginate-immobilized Shewanella oneidensis MR-1. *Biochem. Eng. J.* **2013**, *77*, 183−189.
(61) Park, S.-J.; Park, B.-J.; Ryu, S.-K. Electrochemical treatment on activated carbon fibers for increasing the amount and rate of Cr(VI) adsorption. *Carbon* **1999**, *37*, 1223−1226.
(62) Zheng, W.; Hu, J.; Han, Z.; Wang, Z.; Zheng, Z.; Langer, J.; Economy, J. Synthesis of porous carbon fibers with strong anion exchange functional groups. *Chem. Commun.* **2015**, *51*, 9853−9856.
(63) Zheng, W.; Hu, J.; Han, Z.; Diesel, E.; Wang, Z.; Zheng, Z.; Ba, C.; Langer, J.; Economy, J. Interactions of Cr(VI) with hybrid anion exchange/porous carbon fibers in aqueous solution at natural pH. *Chem. Eng. J.* **2016**, *287*, 54−61.
(64) Li, Y.; Wu, X.; Song, J.; Li, J.; Shao, Q.; Cao, N.; Lu, N.; Guo, Z. Reparation of recycled acrylonitrile-butadiene-styrene by pyromellitic dianhydride: Reparation performance evaluation and property analysis. *Polymer* **2017**, *124*, 41−47.
(65) Huang, L.; Zhou, S.; Jin, F.; Huang, J.; Bao, N. Characterization and mechanism analysis of activated carbon fiber felt-stabilized nanoscale zero-valent iron for the removal of Cr(VI) from aqueous solution. *Colloids Surf., A* **2014**, *447*, 59−66.
(66) Mitra, P.; Sarkar, D.; Chakrabarti, S.; Dutta, B. K. Reduction of hexa-valent chromium with zero-valent iron: batch kinetic studies and rate model. *Chem. Eng. J.* **2011**, *171*, 54−60.
(67) Zhang, L.-H.; Sun, Q.; Liu, D.-H.; Lu, A.-H. Magnetic hollow carbon nanospheres for removal of chromium ions. *J. Mater. Chem. A* **2013**, *1*, 9477−9483.
(68) Zhu, J. H.; Pallavkar, S.; Chen, M. J.; Yerra, N.; Luo, Z. P.; Colorado, H. A.; Lin, H. F.; Haldolaarachchige, N.; Khasanov, A.; Ho, T. C.; Young, D. P.; Wei, S. Y.; Guo, Z. H. Magnetic carbon nanostructures: microwave energy-assisted pyrolysis vs. conventional pyrolysis. *Chem. Commun.* **2013**, *49*, 258−260.
(69) Qiu, B.; Wang, Y.; Sun, D.; Wang, Q.; Zhang, X.; Weeks, B. L.; O'Connor, R.; Huang, X.; Wei, S.; Guo, Z. Cr(VI) removal by magnetic carbon nanocomposites derived from cellulose at different carbonization temperatures. *J. Mater. Chem. A* **2015**, *3*, 9817−9825.
(70) Jing, G.; Zhou, Z.; Song, L.; Dong, M. Ultrasound enhanced adsorption and desorption of chromium (VI) on activated carbon and polymeric resin. *Desalination* **2011**, *279*, 423−427.
(71) Zhang, W.-B.; Deng, M.; Sun, C.-X.; Wang, S.-B. Ultrasound-Enhanced Adsorption of Chromium(VI) on Fe3O4Magnetic Particles. *Ind. Eng. Chem. Res.* **2014**, *53*, 333−339.
(72) Xiang, J.; Li, J.; Zhang, X.; Ye, Q.; Xu, J.; Shen, X. Magnetic carbon nanofibers containing uniformly dispersed Fe/Co/Ni nanoparticles as stable and high-performance electromagnetic wave absorbers. *J. Mater. Chem. A* **2014**, *2*, 16905−16914.
(73) Xiang, J.; Zhang, X.; Ye, Q.; Li, J.; Shen, X. Synthesis and characterization of FeCo/C hybrid nanofibers with high performance of microwave absorption. *Mater. Res. Bull.* **2014**, *60*, 589−595.
(74) Qin, X.-H.; Yang, E.-L.; Li, N.; Wang, S.-Y. Effect of different salts on electrospinning of polyacrylonitrile (PAN) polymer solution. *J. Appl. Polym. Sci.* **2007**, *103*, 3865−3870.
(75) Qu, H.; Wei, S.; Guo, Z. Coaxial electrospun nanostructures and their applications. *J. Mater. Chem. A* **2013**, *1*, 11513.
(76) Zong, X.; Kim, K.; Fang, D.; Ran, S.; Hsiao, B. S.; Chu, B. Structure and process relationship of electrospun bioabsorbable nanofiber membranes. *Polymer* **2002**, *43*, 4403−4412.
(77) Tan, S. H.; Inai, R.; Kotaki, M.; Ramakrishna, S. Systematic parameter study for ultra-fine fiber fabrication via electrospinning process. *Polymer* **2005**, *46*, 6128−6134.
(78) Wen, Z.; Ci, S.; Zhang, F.; Feng, X.; Cui, S.; Mao, S.; Luo, S.; He, Z.; Chen, J. Nitrogen-Enriched Core-Shell Structured Fe/Fe_3C-C Nanorods as Advanced Electrocatalysts for Oxygen Reduction Reaction. *Adv. Mater.* **2012**, *24*, 1399−1404.
(79) Cao, Y.; Yu, H.; Tan, J.; Peng, F.; Wang, H.; Li, J.; Zheng, W.; Wong, N.-B. Nitrogen-, phosphorous- and boron-doped carbon nanotubes as catalysts for the aerobic oxidation of cyclohexane. *Carbon* **2013**, *57*, 433−442.
(80) Heremans, J.; Rahim, I.; Dresselhaus, M. Thermal conductivity and Raman spectra of carbon fibers. *Phys. Rev. B: Condens. Matter Mater. Phys.* **1985**, *32*, 6742.
(81) Wang, Y.; Serrano, S.; Santiago-Aviles, J. J. Raman characterization of carbon nanofibers prepared using electrospinning. *Synth. Met.* **2003**, *138*, 423−427.
(82) Zhong, G.; Wang, H.; Yu, H.; Peng, F. Nitrogen doped carbon nanotubes with encapsulated ferric carbide as excellent electrocatalyst for oxygen reduction reaction in acid and alkaline media. *J. Power Sources* **2015**, *286*, 495−503.
(83) Mills, P.; Sullivan, J. A study of the core level electrons in iron and its three oxides by means of X-ray photoelectron spectroscopy. *J. Phys. D: Appl. Phys.* **1983**, *16*, 723.
(84) Hawn, D. D.; DeKoven, B. M. Deconvolution as a correction for photoelectron inelastic energy losses in the core level XPS spectra of iron oxides. *Surf. Interface Anal.* **1987**, *10*, 63−74.
(85) Chen, W.; Pan, X.; Willinger, M.-G.; Su, D. S.; Bao, X. Facile autoreduction of iron oxide/carbon nanotube encapsulates. *J. Am. Chem. Soc.* **2006**, *128*, 3136−3137.
(86) Li, Y.; Zhu, S.; Liu, Q.; Chen, Z.; Gu, J.; Zhu, C.; Lu, T.; Zhang, D.; Ma, J. N-doped porous carbon with magnetic particles formed in situ for enhanced Cr(VI) removal. *Water Res.* **2013**, *47*, 4188−4197.
(87) Qiu, B.; Guo, J.; Zhang, X.; Sun, D.; Gu, H.; Wang, Q.; Wang, H.; Wang, X.; Zhang, X.; Weeks, B. L.; Guo, Z.; Wei, S. Polyethylenimine facilitated ethyl cellulose for hexavalent chromium removal with a wide pH range. *ACS Appl. Mater. Interfaces* **2014**, *6*, 19816−24.
(88) Li, Y.; Gao, B.; Wu, T.; Sun, D.; Li, X.; Wang, B.; Lu, F. Hexavalent chromium removal from aqueous solution by adsorption on aluminum magnesium mixed hydroxide. *Water Res.* **2009**, *43*, 3067−3075.
(89) Xie, J. C.; Wang, X. H.; Xu, Q. C. Adsorption of hexavalent chromium on carbon nanotubes: influences of surface chemistry and pore structure. *Mater. Technol.* **2012**, *27*, 337−341.
(90) Deng, S.; Bai, R. Adsorption and desorption of humic acid on aminated polyacrylonitrile fibers. *J. Colloid Interface Sci.* **2004**, *280*, 36−43.
(91) Hu, J.; Lo; Chen, G. Fast Removal and Recovery of Cr(VI) Using Surface-Modified Jacobsite (MnFe2O4) Nanoparticles. *Langmuir* **2005**, *21*, 11173−11179.
(92) Park, S.-J.; Jang, Y.-S.; Shim, J.-W.; Ryu, S.-K. Studies on pore structures and surface functional groups of pitch-based activated carbon fibers. *J. Colloid Interface Sci.* **2003**, *260*, 259−264.
(93) Di Natale, F.; Lancia, A.; Molino, A.; Musmarra, D. Removal of chromium ions form aqueous solutions by adsorption on activated carbon and char. *J. Hazard. Mater.* **2007**, *145*, 381−390.
(94) Gupta, V. K.; Rastogi, A.; Nayak, A. Adsorption studies on the removal of hexavalent chromium from aqueous solution using a low cost fertilizer industry waste material. *J. Colloid Interface Sci.* **2010**, *342*, 135−141.
(95) Zhao, R.; Li, X.; Sun, B.; Shen, M.; Tan, X.; Ding, Y.; Jiang, Z.; Wang, C. Preparation of phosphorylated polyacrylonitrile-based nanofiber mat and its application for heavy metal ion removal. *Chem. Eng. J.* **2015**, *268*, 290−299.
(96) Qiu, B.; Xu, C.; Sun, D.; Wei, H.; Zhang, X.; Guo, J.; Wang, Q.; Rutman, D.; Guo, Z.; Wei, S. Polyaniline coating on carbon fiber fabrics for improved hexavalent chromium removal. *RSC Adv.* **2014**, *4*, 29855.
(97) Yuan, P.; Liu, D.; Fan, M.; Yang, D.; Zhu, R.; Ge, F.; Zhu, J.; He, H. Removal of hexavalent chromium [Cr(VI)] from aqueous solutions

DOI: 10.1021/acs.iecr.7b02835
Ind. Eng. Chem. Res. 2017, 56, 10689−10701

by the diatomite-supported/unsupported magnetite nanoparticles. *J. Hazard. Mater.* **2010**, *173*, 614−621.
(98) Shen, Y. F.; Tang, J.; Nie, Z. H.; Wang, Y. D.; Ren, Y.; Zuo, L. Preparation and application of magnetic Fe3O4 nanoparticles for wastewater purification. *Sep. Purif. Technol.* **2009**, *68*, 312−319.
(99) Gu, H. B.; Rapole, S. B.; Huang, Y. D.; Cao, D. M.; Luo, Z. P.; Wei, S. Y.; Guo, Z. H. Synergistic interactions between multi-walled carbon nanotubes and toxic hexavalent chromium. *J. Mater. Chem. A* **2013**, *1*, 2011−2021.
(100) Chen, C. L.; Zhang, J.; Zhang, B. S.; Yu, C. L.; Peng, F.; Su, D. S. Revealing the enhanced catalytic activity of nitrogen-doped carbon nanotubes for oxidative dehydrogenation of propane. *Chem. Commun.* **2013**, *49*, 8151−8153.

DOI: 10.1021/acs.iecr.7b02835
Ind. Eng. Chem. Res. 2017, 56, 10689−10701